Machine learning for thermal transport and phonon high-order anharmonicity in high thermal conductivity materials: A case study in boron arsenide

Lingyun Dai,* Man Li,* and Yongjie Hu†
School of Engineering and Applied Science, University of California, Los Angeles, Los Angeles, California 90095, USA

(Received 2 November 2024; accepted 4 April 2025; published 25 April 2025)

Materials with high thermal conductivity are at the forefront of research in advancing thermal management, as benchmarked by the recent discovery of cubic BAs. In this study, we utilized BAs as a prototype material to assess the predictive capabilities of a machine learning approach for thermal transport, particularly in scenarios where high-order phonon anharmonicity plays a crucial role. We developed a training methodology for the moment tensor potential based on *ab initio* molecular dynamics, which provides accurate predictions of atomic energies, forces, stresses, phonon dispersion relations, elastic modulus, and thermal expansion coefficients. Our approach yields quantitative predictions of thermal conductivity and phonon mean free paths, closely matching first-principles calculations and experimental measurements under varied conditions and size confinements. The predictions of pressure-dependent thermal conductivity, taking into account complex interactions from phonon anharmonicity, isotope scattering, and defect scattering, reveal intrinsic behavior resulting from competing 3-phonon and 4-phonon processes in high-quality BAs, while also showing weak pressure dependence in samples dominated by defects. This study explores the feasibility of using machine learning for simulating high-order phonon scattering and demonstrates its potential as a high-throughput computational approach in advancing thermal management solutions.

DOI: 10.1103/PhysRevMaterials.9.045403

I. INTRODUCTION

Heat dissipation poses a significant challenge in modern electronics, as elevated temperatures can adversely affect system performance, reliability, and lifespan [1–8]. In response, the development of materials with high thermal conductivity has emerged as a forefront area of research [1,3,8–21], providing essential components for electronic thermal management. Recent advancements include the experimental development of compound semiconductors [3,8,10–16] based on first-principles theory calculations [17–26]. Notably, boron phosphide [10] has shown an isotropic thermal conductivity of 500 W/mK and boron arsenide (BAs) [3,8,13,16] has achieved 1300 W/mK. The thermal conductivity of BAs is more than three times that of industrial benchmarks like copper and silicon carbide, both around 400 W/mK, and twice that of cubic boron nitride. Additionally, the mechanical and thermophysical properties of BAs match well with power semiconductors [16], making it well suitable for electronics applications. The recent integration of BAs with gallium nitride (GaN) high-electron-mobility transistors (HEMTs) [11] and flexible thermal interfaces [12] mark a significant stride towards its implementation in thermal management devices, demonstrating lower thermal boundary resistance and better cooling performance compared to diamond or silicon carbide. These remarkable thermal properties of BAs have solidified its role in developing efficient cooling technologies. Further, BAs, with its distinctive phonon dispersion, serves as an exemplary material for investigating high-order anharmonicity and novel phonon physics [13,21]. In this context, the involvement of 4-phonon scattering, along with the traditionally acknowledged 3-phonon scattering, forms more complicated contributions of these processes. These recent advancements underscore the predictive power of first-principles calculations based on density functional theory (DFT) in identifying new materials for electronics thermal management. However, the considerable computational resources and time expenses required by first-principles atomistic calculations may pose challenges for future explorations of complex materials, device structures, and high-throughput evaluations.

In this study, we examined machine learning and its prediction performance for thermal transport and phonon high-order anharmonicity in high thermal conductivity materials, using BAs as a case study. Machine learning (ML) has been extensively utilized in diverse domains such as image recognition, social media analytics, gaming, autonomous driving, and real-time language translation, while it is at a relatively early stage for thermal transport and thermal management [27–37]. For materials with high thermal conductivity, further complexity arises from the crucial roles played by high-order anharmonic processes governed by interatomic forces. The intricacies of capturing the nuances of phonon interactions and anharmonic behaviors in such materials raise questions about the feasibility of achieving satisfactory training outcomes. We performed machine learning training to extract potential energy surface including harmonic and high-order anharmonic interactions, based on *ab initio* molecular dynamics data. Harmonic properties (i.e., phonon dispersion relations, elastic modulus) and basic anharmonic properties (i.e., thermal expansion coefficients) are computed first for preliminary evaluation regarding the predictive fidelity of the trained machine learning

*These authors contributed equally to this work.
†Contact author. yhu@seas.ucla.edu

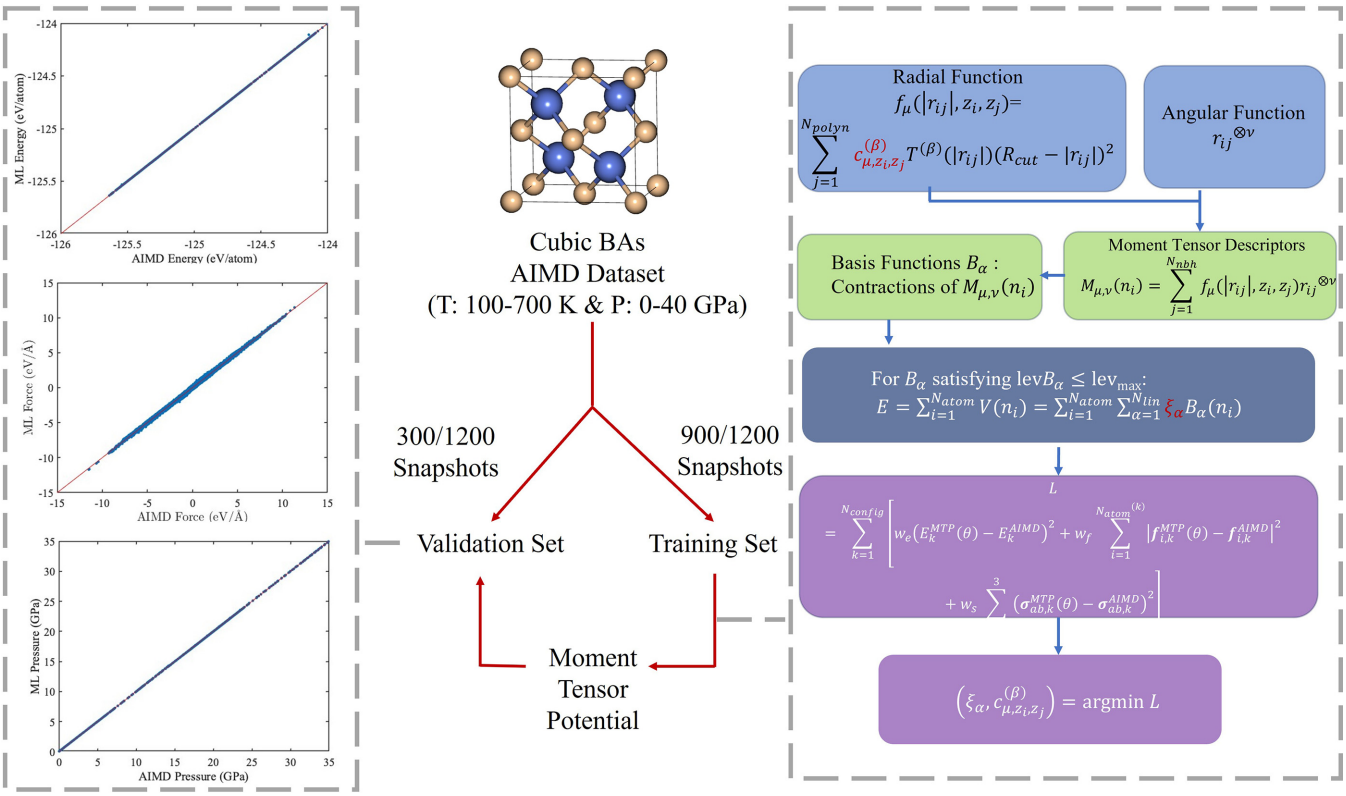

FIG. 1. The development of the machine learning potential in this work. Right in the figure, the training workflow exemplified with moment tensor potential; Left in the figure, the comparison of energy, force, and pressure between machine learning predictions and *ab-initio* molecular dynamics (AIMD) data. The input variables for moment tensor potential are the coefficients ξ_α and $c^{(\beta)}_{\mu,\mathrm{zi,zj}}$ for respective basis functions, as highlighted in red.

potential. Further, we combined machine learning potential with the Boltzmann transport question (BTE) to construct the modeling of 3-phonon, 4-phonon, isotope and defect scatterings with dependence on varied temperatures, high hydrostatic pressures, and confinement sizes. The predicted results reveal competing behaviors arising from high-order anharmonic processes, consistent with first-principles DFT calculations and experimental measurements of BAs, and uncover new properties under varied conditions. Our study affirms the applicability of the machine learning approach for thermal modeling and device analysis when high-order anharmonicity processes, providing high throughput capability for thermal management implementations.

II. DEVELOPMENT OF THE MACHINE LEARNING POTENTIAL

The training framework is illustrated in Fig. 1. We develop the training and validation datasets through *ab initio* molecular dynamics (AIMD) simulations, which can accurately calculate the interatomic interactions using quantum mechanics [38–40]. The system comprises a 512-atom supercell, built from a $4\times4\times4$ expansion of an 8-atom conventional unit cell. The AIMD simulations span a range of hydrostatic pressures from 0 to 40 GPa and temperatures from 100 K to 700 K. The norm-conserving pseudopotential is used with Perdew-Zunger exchange-correlation functional, with a kinetic energy cutoff set at 100 Ry and Γ point sampling. The electronic convergence criterion is controlled at 1×10^{-8} Ry. These parameters ensure the atom-wise force converged within 1×10^{-5} eV/A. The timestep is 1 fs and the AIMD configurations are sampled every five timesteps. 1200 snapshots in total, with atomic energies, forces, and stresses are collected in the end. We partition this dataset randomly into two subsets, a training dataset containing 900 snapshots and a validation dataset containing the remaining 300 snapshots for evaluating the predictive capability of the model. The simulations are performed using the Quantum Espresso package [41,42].

For the concept demonstration, moment tensor potential (MTP) [42] is used for developing machine learning modeling as MTP has been tested to show high accuracy for force and energy prediction with a balanced high speed regarding training and later-on molecular simulations, in comparison with other widely used machine learning potentials including Gaussian Approximation Potential (GAP), Neural Network Potential (NNP), Spectral Neighbor Analysis Potential (SNAP), and quadratic Spectral Neighbor Analysis Potential (qSNAP) [43]. This is due to its straightforward linear regression structure, which is much simpler compared to sophisticated architectures (e.g., multilayer perceptron in neural networks) as in some other machine learning potentials. Notably, MTP have also been tested for thermal properties prediction in varied phases of materials, such as α and β phases of Ga_2O_3 [44], Tl_9SbTe_6 [45] and FLiBe [46], $La_2Zr_2O_7$ [47]. MTP is a local environment-based potential

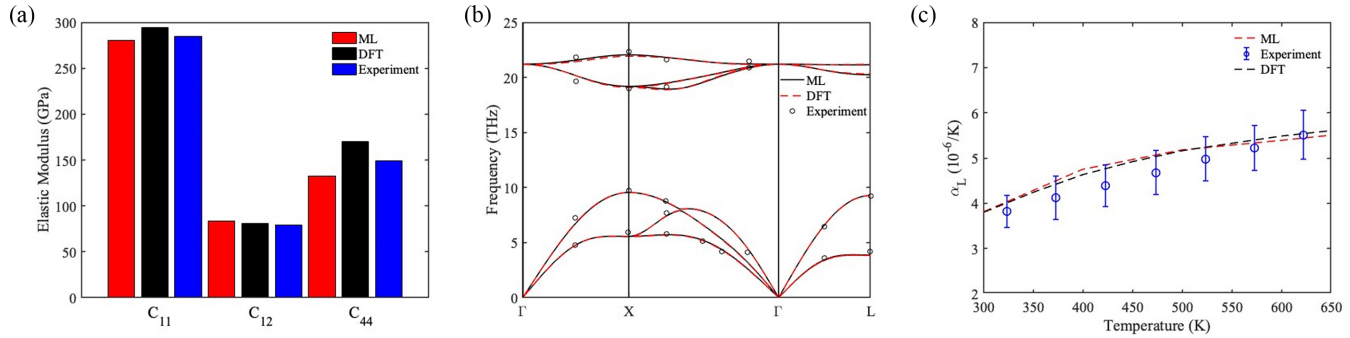

FIG. 2. Machine learning predictions on elastic modulus, dispersion relations, and thermal expansion coefficient of BAs. (a) The predicted elastic modulus C_{11}, C_{12} and C_{44}, in comparison with their DFT calculations and experimental measurements [16]. (b) The predicted phonon dispersion relations along $\Gamma - X - \Gamma - L$ by machine learning, in comparison with DFT results and neutron scattering experimental data [13]. (c) The predicted thermal expansion coefficients from 300 to 650 K by machine learning, in comparison with DFT calculations and experimental measurements [16].

where the total energy of the system is the summation of the contributions from all N atoms within the system. Each atom's contribution is intricately determined by the specific characteristics of its atomic neighborhood environment, n_i, through the relative positions and atomic types of neighboring atoms within a given cutoff distance. Every such contribution term $V(n_i)$ can be expanded through a linear combination of a set of basis functions $B_\alpha(n_i)$, each weighted by coefficients ξ_α. The functional form of the basis functions is resolved by the possible contractions of moment tensor descriptors $M_{\mu,\nu}(n_i)$ of varied levels of complexity, where $M_{\mu,\nu}(n_i)$ involves vector outer product as angular part $r_{ij}^{\otimes\nu}$ and smoothed polynomial functions-based expansion $f_\mu(|r_{ij}|, z_i, z_j)$ as radial part over each atomic pair (i, j) within the neighborhood of atom i. Given a predetermined level of the momentum tensor descriptor, which specifies the tensor rank of the angular component and the number of the radial functions for the radial component, all the MTP basis functions below this level are utilized for the construction of the potential. To find the MTP parameters, $\boldsymbol{\theta}$, (i.e., the coefficients for basis functions B_α and for polynomials in the radial part of moment tensor descriptors $c_{\mu,z_i,z_j}^{(\beta)}$), the objective function L is defined as the weighted squared error across all energies/forces/stresses between the MTP predictions and the AIMD data and minimized numerically using the Broyden-Fletcher-Goldfarb-Shanno algorithm. The parameters at the local minimum are considered the optimized set. Both the training and the validation of the MTP model are performed using the MLIP package [42].

III. RESULTS AND DISCUSSIONS

A. Accuracy on the trained machine learning potential

To test the accuracy of the trained machine learning potential (MLP), we present a comparison between ML predictions and AIMD values concerning atomic energies, forces, and system pressure, respectively, regarding the validation dataset. As shown in Fig. 1, the close alignment of most data points along the diagonal line is indicative of an excellent agreement between the MTP predictions and the actual AIMD results. Statistically, the root-mean-square error for energy is 2.38 meV/atom, for atomic force is 41.6 meV/Å, and for pressure is 0.05 GPa, respectively. These quantitative metrics, comparable to the typical error level [39,40,48–50] as many other machine learning potentials in the literature, underscore the fidelity of our MTP model in describing atomic interactions nearly on the same level as DFT calculations, establishing a strong foundation for its application on material property computation.

B. Harmonic properties (elastic modulus and phonon dispersion

We leverage the trained MLP on material property predictions starting from the harmonic properties, i.e., elastic modulus and phonon dispersion relations. To calculate elastic modulus, we build a 5×5×5 supercell and apply periodic boundary conditions. The elastic modulus is computed by relating applied strain and the resulting stress tensors in the limit of infinitesimal deformation. As presented in Fig. 2(a), the predicted elastic modulus C_{11}, C_{12}, and C_{44} from MLP show good consistency with the experimental measurement of BAs crystals [16] with a maximum percentage difference of around 11.4%. Next, the phonon dispersion relations at zero pressure, which embed the spectrum of existing phonon modes and deliver the crucial information (i.e., group velocity, scattering phase space) in thermal transport, is determined. Interatomic force constants calculations are completed on supercells containing 216 atoms using ALAMODE package [51]. We generate sets of irreducible displacements of the second-order interactions and calculated the atomic forces from the MLP and DFT. The force-displacement datasets obtained are then utilized to fit force constants, which are the inputs for the diagonalization of the dynamical matrix and the resulting phonon dispersion relations. The phonon dispersion of BAs by MLP prediction (solid line) is plotted together with DFT calculation (dashed line) and neutron scattering experiment [13] (symbols) in Fig. 2(b): For the full dispersion along $\Gamma - X - \Gamma - L$ path, the MLP prediction shows very good agreement with DFT and experiments.

C. Anharmonic thermal expansion

To evaluate MLP's anharmonic prediction, we first look at the thermal expansion coefficient α_L from 300 K to 600 K at zero pressure. MD simulations are performed to calculate the

thermal expansion coefficient α_L using the LAMMPS package [52] with a timestep of 1fs. The simulation box is relaxed in the NPT ensemble (constant particle number, pressure, and temperature) for 1.5 ns at temperatures from 200 K to 700 K with a step size of 100 K. The thermal expansion coefficient at a certain temperature T is then calculated numerically invoking central difference, using the averaged lattice constant L at equilibrium over the last 500 ps.

$$\alpha_L = \frac{1}{L}\frac{dL}{dT} \tag{1}$$

As shown in Fig. 2(c), the MLP calculations (dashed line) show consistency with the experimentally measured thermal expansion coefficients of BAs [16].

D. Temperature-dependent thermal transport under varied phonon anharmonicities

As a further step, we apply the ML approach to model more complex phonon-phonon interactions that involve high-order anharmonicity. In general, thermal transport properties are encoded by varied orders of phonon anharmonicities. For most common materials, anharmonicity based on 3-phonon processes is sufficient to describe thermal conductivity near ambient conditions while higher-order processes such as 4-phonon processes can be negligible [53]. However, BAs represents an ideal platform to study high-order anharmonicity. Due to its unique phonon dispersions and resulted low scattering rates, both 3-phonon and 4-phonon are confirmed to contribute substantially to thermal conductivity even at room temperature from experiment [3,13]. First, we calculate the temperature-dependent thermal conductivity of BAs based on the BTE framework using MLP force constants, by considering up to fourth-order anharmonicity and isotope scattering. Third- and fourth -order force constants are determined based on the supercells containing 216 atoms, where the interactions with up to the 5^{th} and 2^{nd} nearest neighbors inside the supercell, are considered respectively.

Notably, the majority of computation cost for high-order phonon processes calculation lies in the evaluation of varying orders of interatomic force constants. Here we compare the computational cost needed for force constants calculation from first principles and our machine learning potential. Using Pittsburgh Supercomputing Center (PSC) bridges-2 infrastructure, based on a parallel environment of 128 CPU cores, the average time needed for atomistic force calculation for a displaced configuration composed of a $3\times3\times3$ supercell with 216 atoms inside is around 81 min from DFT. By contrast, the machine learning potential only requires less than 1 sec for a serial setting on the same displaced configuration, equivalently showing more than 600 000 times acceleration per core. Even taking into account the time spent in collecting *ab initio* molecular dynamics data (i.e., ∼240 hours for 128 cores in parallel) and that in training (i.e., ∼12 hours for a serial node), the actual total amount of time from the beginning to obtaining high-accuracy varying-order force constants is still around 3 times faster than DFT calculation. This remarkable speed-up demonstrates tremendous appeal for its application in physical processes with high-order anharmonicities.

To obtain temperature-dependent thermal conductivity of BAs, the linearized phonon BTE is solved fully iteratively, where 3-phonon scattering, 4-phonon scattering, and isotope scattering are included using a modified BTE solver in the ALAMODE package. A k mesh of $15\times15\times15$ is used. As shown in Fig. 3(a), MLP is used to predict thermal conductivity under the considerations of 3-phonon only and both 3- and 4-phonon processes, respectively. The 3-phonon prediction shows an overestimation of the thermal conductivity; After the inclusion of both 3- and 4-phonon scattering, the ML prediction verifies the substantial contribution from the 4-phonon processes and the reduction in thermal conductivity. The ML results show consistency with experimental measurements [3,13] and DFT [17]. In addition, we apply the ML approach to model size-dependent thermal conductivity as a result of nanostructuring or quasiballistic thermal transport due to confined heating profiles. The calculated phonon mean free path spectrum for accumulated thermal conductivity at 300 K, is plotted in Fig. 3(b), with the machine learning approach and DFT respectively, showing close agreement. Experimentally, quasiballistic thermal transport, related to phonon mean free path spectra, can be observed by measuring size-dependent thermal conductivity using varied heat spot sizes, more detailed experimental methods and quantitative analyses of phonon mean free path spectral contributions in three dimensions to size-dependent thermal conductivity can be found in our recent reports [3,26,54]. By plotting the modeling and experimental results together, the ML-based calculations provide reasonable qualifications on the phonon size effect. The machine learning approach provides computation convenience for future evaluations on electronics heat dissipations, especially for nanoscale devices, where the size effect is critical in thermal transport analysis exemplified by the complicated ballistic to diffusive and interface transport in heterogeneous structures of BAs integrated GaN HEMTs [11].

E. Pressure-dependent thermal transport: competition among phonon anharmonicities of varying orders

BAs represents a prototype material to investigate the high-order phonon anharmonicity under extreme conditions. Besides high temperature, recent studies on BAs have verified the competitive interactions between 3-phonon and 4-phonon anharmonic processes under high pressure [13,55]. Here we use a pressure-dependent setting to examine the effectiveness of implementing machine learning on thermal transport with high-order phonon anharmonicity. First, phonon dispersion relations under varied high pressures up to 30 GPa are calculated from MLP force constants. As shown in Fig. 4(a), the ML results are in good agreement with DFT. Then the pressure-dependent thermal conductivity is predicted using MLP by solving the Boltzmann transport equation for relaxed BAs systems under each pressure for every 5 GPa. As shown in Fig. 4(b), under the consideration of the 3-phonon scattering processes, ML-predicted thermal conductivity decreases with pressure. Under the consideration of both 3- and 4-phonon processes, a nonmonotonic trend emerges, and agrees with the experiment and DFT [13,55]. More quantitatively, we analyze the scattering rates of 3- and 4-phonon processes

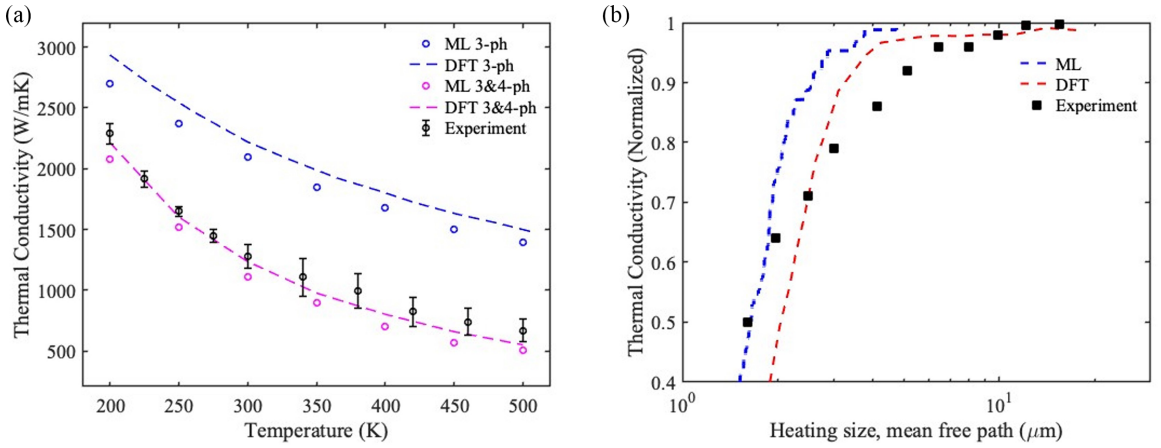

FIG. 3. Machine learning predictions on temperature-dependent thermal conductivity and phonon mean free path spectrum of BAs. (a) The predicted thermal conductivity of BAs by machine learning as a function of temperature, plotted together with DFT calculations and experimental measurements [3,13]. For machine learning and DFT results, computations considering only 3-phonon scattering processes and both 3- and 4-phonon processes are plotted. (b) Phonon mean free path spectrum predicted by machine learning, plotted together with the DFT results and size-dependent experiments at 300 K [3].

as a function of phonon mode frequency, specifically under varied high pressures in Fig. 4(c). The evolution of the intrinsic thermal conductivity in high-quality BAs crystals as a function of pressure is attributed to competing interactions of high-order anharmonic phonon scattering processes, e.g., 3-phonon AAA and 4-phonon AAOO processes as illustrated in Fig. 4(a). At zero pressure, the unique characteristics in BAs phonon dispersion (i.e., large acoustic-optical band gap and bunching of acoustic branches) lead to the strongly restricted 3-phonon scattering channels among three acoustic phonons (AAA) and among acoustic and optical phonons, as well as the unignorable 4-phonon scattering channels involving two acoustic and two optical phonons (AAOO). While 3-phonon scattering generally remains stronger than 4-phonon scattering at zero pressure, as in most materials, 4-phonon scattering rates of acoustic phonons around 5–10 THz, which contribute significantly to thermal transport, are observed to be higher than 3-phonon scattering rates, highlighting the significance of including 4-phonon scattering in thermal conductivity calculation. However, as the pressure increases to 20 GPa, from Fig. 4(a), both optical and longitudinal acoustic branches become hardened while the transverse acoustic branches remain largely unchanged, resulting in expanded phase space for AAA scatterings and reduced phase space for AAOO scatterings. Hence, 4-phonon scattering rates decrease whereas 3-phonon scattering rates continue to increase, yielding comparable strengths between the two scattering mechanisms near 5–10 THz. At an even higher pressure of 30 GPa, 3-phonon scattering rates dominate over 4-phonon scattering rates. This pressure-induced competition between opposing 3-phonon and 4-phonon scattering leads to the observed trend where thermal conductivity increases under lower pressures

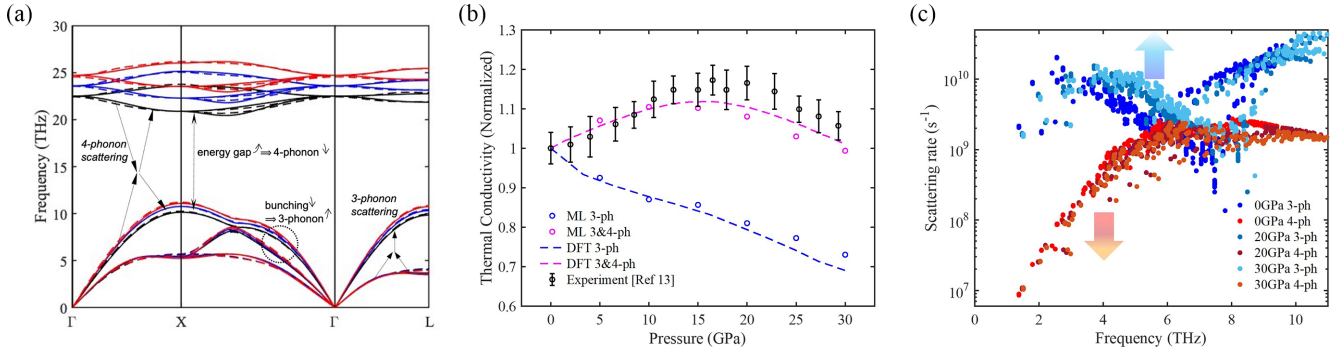

FIG. 4. Machine learning prediction on pressure-dependence phonon dispersion relations and thermal conductivity. (a) Machine learning predicted phonon dispersion relations of BAs along $\Gamma - X - \Gamma - L$ (solid line) under varied hydrostatic pressures: 10 GPa (black), 20 GPa (blue), and 30 GPa (red), plotted together with DFT calculation (dashed line). Inset schematic illustrates the competing interactions from 3-phonon scattering and 4-phonon scattering processes with evolved phonon dispersions under high pressure. (b) Pressure-dependence of thermal conductivity from machine learning, plotted with DFT results and experimental measurements [13]. For machine learning and DFT computations, consideration with only 3-phonon processes and both 3- and 4-phonon processes are presented for comparison. For better illustration, all data are normalized at 0 GPa. (c) Pressure-dependence of 3-phonon (blue) and 4-phonon (red) scattering rates under 0, 20, and 30 GPa. The blue and red arrows show the trend of their variation as the pressure increases.

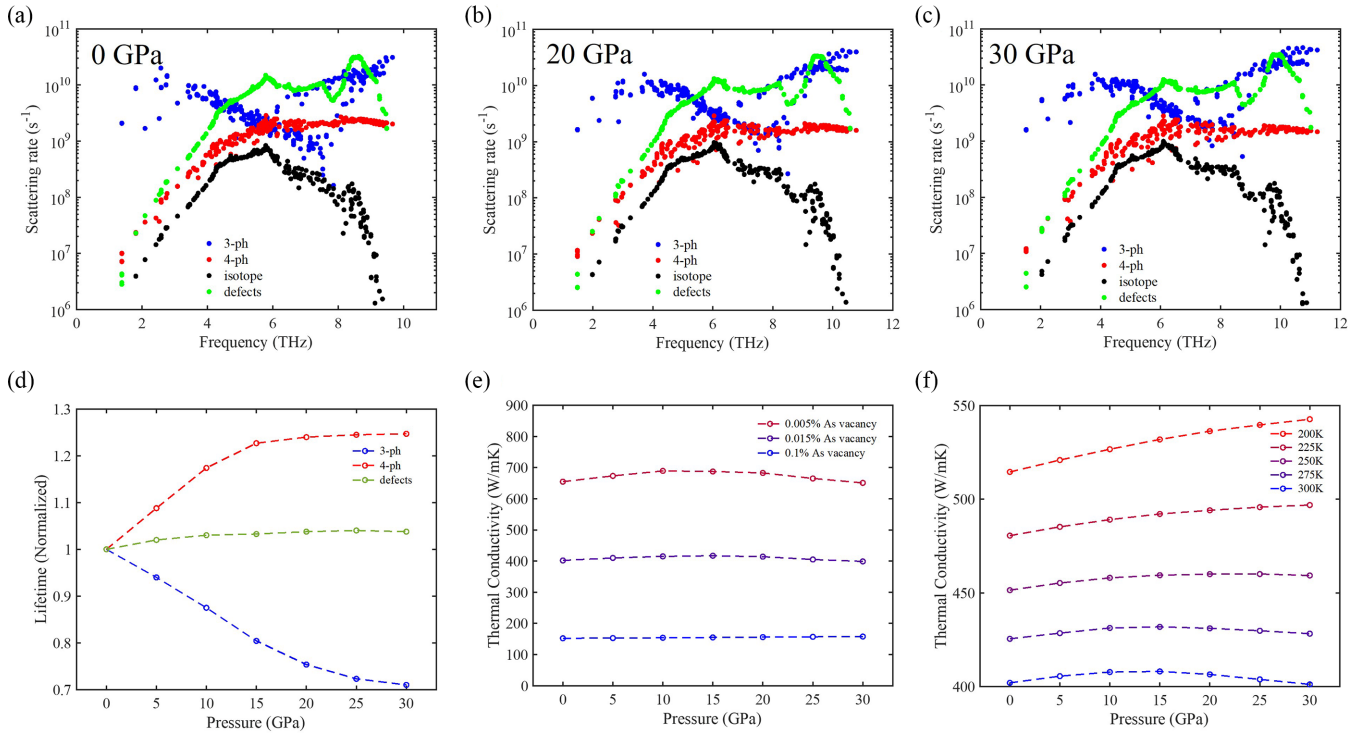

FIG. 5. Machine learning prediction of pressure-dependent phonon scattering rates and thermal conductivity, evaluating the effects of defect scattering and intrinsic anharmonicity involving 3-phonon, 4-phonon, and isotope scattering processes. (a)–(c) The predicted mode-specific scattering rates for 3-phonon, 4-phonon, isotope, and defect scattering in natural abundance BAs with 0.015% As vacancy at 0 GPa, 20 GPa, and 30 GPa, respectively. (d) The pressure dependence of normalized phonon lifetime averaged over all modes due to 3-phonon, 4-phonon, and defect scattering. (e) Pressure dependence of thermal conductivity for BAs samples where defect scattering is non-negligible, with varied As vacancy concentrations. (f) Pressure dependence of thermal conductivity for defected BAs at varied temperatures, modeled with an As vacancy of 0.015%.

when 4-phonon processes are more influential and decreases as 3-phonon scattering becomes the predominant mechanism.

F. Role of defects in pressure-modulated thermal transport

Moreover, we have evaluated the impact of defect scattering on the pressure-dependent thermal conductivity, along with intrinsic 3- and 4-phonon scattering and isotope scattering. Previous work has focused on examining the intrinsic thermal transport in high-quality BAs crystals with minimal defects [13,55], where phonon-phonon interactions dominate and interactions with high-order anharmonicity are presented. However, the potential for thermal management and practical applications also requires an assessment of BAs with defects and semiconductor doping. Here, the ML approach allows for the consideration of defective samples together with intrinsic phonon scattering mechanisms. As shown in Figs. 5(a)–5(c), the mode-specific scattering rates under varied pressures from defects (0.015% As vacancy) are predicted. For comparison, defect scattering could overwhelm phonon-phonon scattering rates, possibly masking the intrinsic competition mechanism of 3-phonon and 4-phonon scattering under high pressure as observed in high-quality BAs crystals. For better illustration, the predicted pressure-dependent effective phonon lifetime (i.e., a weighted average over all phonon modes with their heat capacity and squared velocity as weighting factors) from these three competing mechanisms are plotted respectively in Fig. 5(d), showing a clear contrast in the pressure-dependent trend: Under the relaxation time approximation, 3-phonon and 4-phonon scattering are expected to show a monotonic increase and decrease in lifetime with pressure, respectively. By contrast, the defect scattering lifetime shows a weak dependence on pressure. We attribute these differences in dependence to their distinct scattering physics principles: The dictated point-defect scattering channels, subject to energy conservation by phonon density of states, remain unchanged despite increased pressure, unlike the 3-phonon and 4-phonon processes, where acoustic-optic bandgap opening and reduced acoustic bunching drastically alter the scattering phase space and lead to notable pressure dependence. More quantitatively, ML allows for the evaluation of defect concentrations, and we plot the results in Fig. 5(e). As shown, the pressure dependence of thermal conductivity becomes much weaker as defect concentration increases, for example from 0.005% to 0.015% to 0.1%. Moreover, ML predicts the temperature effect on the samples when defect scattering dominates the thermal conductivity. As presented in Fig. 5(f), below 250 K, the pressure dependence of thermal conductivity in defected BAs shows an increasing trend, different from the nonmonotonic behavior in defect-free BAs. This can be attributed to the hardening of phonon group velocity as pressure increases, where the weakening pressure-induced 3-phonon and 4-phonon competition is further obscured beneath pressure-insensitive defect scattering at lower temperatures. We note that calculations

on samples with higher defect concentrations exhibit a weak pressure dependence in thermal conductivity, which is consistent with recent measurements [56,57]. These results confirm the requirement for high-purity BAs crystals to observe the intrinsic high-order anharmonicity physics and also indicate interesting opportunities to evaluate the effect of defects in thermal transport physics.

IV. CONCLUSION

In summary, we explored the capability of machine learning in predicting thermal transport and high-order anharmonic phonon behaviors in boron arsenide, a material with high thermal conductivity. We utilized the moment tensor potential to analyze the thermal transport properties, particularly focusing on its significant high-order anharmonic effects. Our machine-learning model demonstrates the ability to predict atomic energies, forces, and stresses with an accuracy comparable to DFT calculations. It enabled high-fidelity predictions of elastic moduli, phonon dispersion relations, and thermal expansion coefficients. In terms of thermal conductivity, integrating the Boltzmann Transport Equation with machine learning allowed for the consideration of temperature-dependence, encompassing both 3-phonon and 4-phonon processes, as well as size-dependence resulting from quasiballistic phonon transport. These predictions align well with experimental data and DFT results. Furthermore, our study reveals that with meticulous training, the ML approach can also capture the nonmonotonic pressure dependence that arises from the interplay between 3-phonon and 4-phonon scattering processes, as well as the effects of crystal defects and isotope scattering. This finding suggests that ML offers a viable alternative for modeling complex thermal transport phenomena and multiple anharmonic levels. Additionally, integrating machine learning with other computational tools, such as molecular dynamics and Monte Carlo simulations, could inherently capture various phenomena altogether, such as anharmonic effects, nanostructuring, size-confined quasiballistic thermal transport, temperature-dependent behaviors, as well as the impacts of defects, boundaries, and disorders. This approach offers broader scale and speed advantages compared to traditional first-principles methodologies, for designing effective thermal management solutions and electronic materials.

ACKNOWLEDGMENTS

Y.H. acknowledges support from the National Science Foundation under Grant No. DMR-1753393, an Alfred P. Sloan Research Fellowship under Grant No. FG-2019-11788, Watanabe Excellence in Research Award, and a NIGMS Research Award under Grant No. R35GM147391. For this Account, we used computational and storage services associated with the Hoffman 2 Shared Cluster provided by UCLA Office of Advanced Research Computing's Research Technology Group and the Bridges-2 at Pittsburgh Supercomputing Center through Allocation No. DMR180111 from Advanced Cyberinfrastructure Coordination Ecosystem: Services & Support.

[1] Y. Cui, M. Li, and Y. Hu, Emerging interface materials for electronics thermal management: Experiments, modeling, and new opportunities, J. Mater. Chem. C. Mater. **8**, 10568 (2020).

[2] M. Li, H. Wu, E. M. Avery, Z. Qin, D. P. Goronzy, H. D. Nguyen, T. Liu, P. S. Weiss, and Y. Hu, Electrically gated molecular thermal switch, Science **382**, 585 (2023).

[3] J. S. Kang, M. Li, H. Wu, H. Nguyen, and Y. Hu, Experimental observation of high thermal conductivity in boron arsenide, Science **361**, 575 (2018).

[4] M. M. Waldrop, More than Moore, Nature (London) **530**, 144 (2016).

[5] P. Ball, Feeling the heat: The more that microcircuits are shrunk, the hotter they get. Engineers are on the hunt for ways to cool off computing, Nature (London) **492**, 174 (2012).

[6] S. Chu and A. Majumdar, Opportunities and challenges for a sustainable energy future, Nature (London) **488**, 294 (2012).

[7] Z. Qin, M. Li, J. Flohn, and Y. Hu, Thermal management materials for energy-efficient and sustainable future buildings, Chem. Commun. **57**, 12236 (2021).

[8] M. Li, S. Li, Z. Zhang, C. Su, B. Wong, and Y. Hu, Advancing thermal management technology for power semiconductors through materials and interface engineering, Acc. Mater. Res. (2025), doi:10.1021/accountsmr.4c00349.

[9] O. Bubnova, Thermal release, Nat. Nanotechnol. **13**, 620 (2018).

[10] J. S. Kang, H. Wu, and Y. Hu, Thermal properties and phonon spectral characterization of synthetic boron phosphide for high thermal conductivity applications, Nano Lett. **17**, 7507 (2017).

[11] J. S. Kang, M. Li, H. Wu, H. Nguyen, T. Aoki, and Y. Hu, Integration of boron arsenide cooling substrates into gallium nitride devices, Nat. Electron. **4**, 416 (2021).

[12] Y. Cui, Z. Qin, H. Wu, M. Li, and Y. Hu, Flexible thermal interface based on self-assembled boron arsenide for high-performance thermal management, Nat. Commun. **12**, 1284 (2021).

[13] S. Li, Z. Qin, H. Wu, M. Li, M. Kunz, A. Alatas, A. Kavner, and Y. Hu, Anomalous thermal transport under high pressure in boron arsenide, Nature (London) **612**, 459 (2022).

[14] S. Li, Q. Zheng, Y. Lv, X. Liu, X. Wang, P. Y. Huang, D. G. Cahill, and B. Lv, High thermal conductivity in cubic boron arsenide crystals, Science **361**, 579 (2018).

[15] F. Tian, B. Song, X. Chen, N. K. Ravichandran, Y. Lv, K. Chen, S. Sullivan, J. Kim, Y. Zhou, T.-H. Liu, M. Goni, Z. Ding, J. Sun, G. A. G. U. Gamage, H. Sun, H. Ziyaee, S. Huyan, L. Deng, J. Zhou, A. J. Schmidt *et al.*, Unusual high thermal conductivity in boron arsenide bulk crystals, Science **361**, 582 (2018).

[16] J. S. Kang, M. Li, H. Wu, H. Nguyen, and Y. Hu, Basic physical properties of cubic boron arsenide, Appl. Phys. Lett. **115**, 122103 (2019).

[17] L. Lindsay, D. A. Broido, and T. L. Reinecke, First-principles determination of ultrahigh thermal conductivity of boron

arsenide: A competitor for diamond? Phys. Rev. Lett. **111**, 025901 (2013).
[18] D. A. Broido, L. Lindsay, and T. L. Reinecke, *Ab initio* study of the unusual thermal transport properties of boron arsenide and related materials, Phys. Rev. B **88**, 214303 (2013).
[19] H. Wu, H. Fan, and Y. Hu, *Ab initio* determination of ultrahigh thermal conductivity in ternary compounds, Phys. Rev. B **103**, L041203 (2021).
[20] H. Fan, H. Wu, L. Lindsay, and Y. Hu, *Ab initio* investigation of single-layer high thermal conductivity boron compounds, Phys. Rev. B **100**, 085420 (2019).
[21] H. Wu, Z. Qin, S. Li, L. Lindsay, and Y. Hu, Nonperturbative determination of isotope-induced anomalous vibrational physics, Phys. Rev. B **108**, L140302 (2023).
[22] T. Feng, L. Lindsay, and X. Ruan, Four-phonon scattering significantly reduces intrinsic thermal conductivity of solids, Phys. Rev. B **96**, 161201(R) (2017).
[23] N. Mingo and D. A. Broido, Lattice thermal conductivity crossovers in semiconductor nanowires, Phys. Rev. Lett. **93**, 246106 (2004).
[24] A. Ward, D. A. Broido, D. A. Stewart, and G. Deinzer, *Ab initio* theory of the lattice thermal conductivity in diamond, Phys. Rev. B **80**, 125203 (2009).
[25] K. Esfarjani, G. Chen, and H. T. Stokes, Heat transport in silicon from first-principles calculations, Phys. Rev. B **84**, 085204 (2011).
[26] Y. Hu, L. Zeng, A. J. Minnich, M. S. Dresselhaus, and G. Chen, Spectral mapping of thermal conductivity through nanoscale ballistic transport, Nat. Nanotechnol. **10**, 701 (2015).
[27] M. Li, L. Dai, and Y. Hu, Machine learning for harnessing thermal energy: From materials discovery to system optimization, ACS Energy Lett. **7**, 3204 (2022).
[28] X. Qian and R. Yang, Machine learning for predicting thermal transport properties of solids, Mater. Sci. Eng.: R: Rep. **146**, 100642 (2021).
[29] S. Ju, S. Shimizu, and J. Shiomi, Designing thermal functional materials by coupling thermal transport calculations and machine learning, J. Appl. Phys. **128**, 161102 (2020).
[30] H. Wei, H. Bao, and X. Ruan, Perspective: Predicting and optimizing thermal transport properties with machine learning methods, Energy and AI **8**, 100153 (2022).
[31] X. Wan, W. Feng, Y. Wang, H. Wang, X. Zhang, C. Deng, and N. Yang, Materials discovery and properties prediction in thermal transport via materials informatics: A mini review, Nano Lett. **19**, 3387 (2019).
[32] T. Wang, C. Zhang, H. Snoussi, and G. Zhang, Machine learning approaches for thermoelectric materials research, Adv. Funct. Mater. **30**, 1906041 (2020).
[33] Y. Ouyang, C. Yu, G. Yan, and J. Chen, Machine learning approach for the prediction and optimization of thermal transport properties, Front. Phys., **16**, 43200 (2021).
[34] M. T. Hughes, G. Kini, and S. Garimella, Status, challenges, and potential for machine learning in understanding and applying heat transfer phenomena, J. Heat Transfer **143**, 120802 (2021).
[35] R. Li, E. Lee, and T. Luo, A unified deep neural network potential capable of predicting thermal conductivity of silicon in different phases, Mater. Today Phys. **12**, 100181 (2020).
[36] X. Wan, D. Ma, D. Pan, L. Yang, and N. Yang, Optimizing thermal transport in graphene nanoribbon based on phonon resonance hybridization, Mater. Today Phys. **20**, 100445 (2021).
[37] L. Yang, X. Wan, D. Ma, Y. Jiang, and N. Yang, Maximization and minimization of interfacial thermal conductance by modulating the mass distribution of the interlayer, Phys. Rev. B **103**, 155305 (2021).
[38] X. Qian, S. Peng, X. Li, Y. Wei, and R. Yang, Thermal conductivity modeling using machine learning potentials: Application to crystalline and amorphous silicon, Mater. Today Phys. **10**, 100140 (2019).
[39] H. Liu, X. Qian, H. Bao, C. Y. Zhao, and X. Gu, High-temperature phonon transport properties of SnSe from machine-learning interatomic potential, J. Phys.: Condens. Matter **33**, 405401 (2021).
[40] R. Li, Z. Liu, A. Rohskopf, K. Gordiz, A. Henry, E. Lee, and T. Luo, A deep neural network interatomic potential for studying thermal conductivity of β-Ga_2O_3, Appl. Phys. Lett. **117**, 152102 (2020).
[41] P. Giannozzi, S. Baroni, N. Bonini, M. Calandra, R. Car, C. Cavazzoni, D. Ceresoli, G. L Chiarotti, M. Cococcioni, I. Dabo, A. D. Corso, S. de Gironcoli, S. Fabris, G. Fratesi, R. Gebauer, U. Gerstmann, C. Gougoussis, A. Kokalj, M. Lazzeri, L. Martin-Samos *et al.*, QUANTUM ESPRESSO: A modular and open-source software project for quantum simulations of materials, J. Phys.: Condens. Matter **21**, 395502 (2009).
[42] E. Podryabinkin, K. Garifullin, A. Shapeev, and I. Novikov, MLIP-3: Active learning on atomic environments with moment tensor potentials, J. Chem. Phys. **159**, 084112 (2023).
[43] Y. Zuo, C. Chen, X. Li, Z. Deng, Y. Chen, J. Behler, G. Csányi, A. V. Shapeev, A. P. Thompson, M. A. Wood, and S. P. Ong, Performance and cost assessment of machine learning interatomic potentials, J. Phys. Chem. A **124**, 731 (2020).
[44] N. Rybin and A. Shapeev, A moment tensor potential for lattice thermal conductivity calculations of α and β phases of Ga_2O_3, J. Appl. Phys. **135**, 205108 (2024).
[45] Y. Hao, Y. Zuo, J. Zheng, W. Hou, H. Gu, X. Wang, X. Li, J. Sun, X. Ding, and Z. Gao, Machine learning for predicting ultralow thermal conductivity and high *ZT* in complex thermoelectric materials, ACS Appl. Mater. Interfaces **16**, 47866 (2024).
[46] S. Attarian, D. Morgan, and I. Szlufarska, Thermophysical properties of FLiBe using moment tensor potentials, J. Mol. Liq. **368**, 120803 (2022).
[47] H. Zhou, J. Tiwari, and T. Feng, Understanding the flat thermal conductivity of $La_2Zr_2O_7$ at ultrahigh temperatures, Phys. Rev. Mater. **8**, 043804 (2024).
[48] X. Qian and R. Yang, Temperature effect on the phonon dispersion stability of zirconium by machine learning driven atomistic simulations, Phys. Rev. B **98**, 224108 (2018).
[49] C. Cui, Y. Zhang, T. Ouyang, C. Tang, C. He, J. Li, M. Chen, and J. Zhong, Machine learning interatomic potentials as efficient tools for obtaining reasonable phonon dispersions and accurate thermal conductivity: A case study of typical two-dimensional materials, Appl. Phys. Lett. **123**, 152201 (2023).
[50] H. Zhang, X. Gu, Z. Fan, and H. Bao, Vibrational anharmonicity results in decreased thermal conductivity of amorphous HfO_2 at high temperature, Phys. Rev. B **108**, 045422 (2023).

[51] T. Tadano, Y. Gohda, and S. Tsuneyuki, Anharmonic force constants extracted from first-principles molecular dynamics: Applications to heat transfer simulations, J. Phys.: Condens. Matter **26**, 225402 (2014).

[52] A. P. Thompson, H. M. Aktulga, R. Berger, D. S. Bolintineanu, W. M. Brown, P. S. Crozier, P. J. in't Veld, A. Kohlmeyer, S. G. Moore, T. D. Nguyen, R. Shan, M. J. Stevens, J. Tranchida, C. Trott, and S. J. Plimpton, LAMMPS–A flexible simulation tool for particle-based materials modeling at the atomic, meso, and continuum scales, Comput. Phys. Commun. **271**, 108171 (2022).

[53] L. Lindsay and D. A. Broido, Three-phonon phase space and lattice thermal conductivity in semiconductors, J. Phys.: Condens. Matter **20**, 165209 (2008).

[54] C. Su, H. Wu, L. Dai, Z. Zhang, S. Li, and Y. Hu, Nonclassical heat transfer and recent progress, ASME J. Heat Mass Transfer **147**, 032502 (2025).

[55] N. K. Ravichandran and D. Broido, Non-monotonic pressure dependence of the thermal conductivity of boron arsenide, Nat. Commun. **10**, 827 (2019).

[56] Y. Zhou, W. P. Hsieh, C. C. Chen, X. Meng, F. Tian, Z. Ren, L. Shi, J. F. Lin, and Y. Wang, Defect-modulated thermal transport behavior of BAs under high pressure, Appl. Phys. Lett. **121**, 121902 (2022).

[57] S. Hou, B. Sun, F. Tian, Q. Cai, Y. Xu, S. Wang, X. Chen, Z. Ren, C. Li, and R. B. Wilson, Thermal conductivity of BAs under pressure, Adv. Electron Mater. **8**, 2200017 (2022).